Applied Physics A (2021) 127:907
https://doi.org/10.1007/s00339-021-05071-x

Applied Physics A
Materials Science & Processing

Enhanced light–matter interaction in a hybrid photonic–plasmonic cavity

Belkıs Gökbulut[1] · Arda Inanç[1] · Gokhan Topcu[2] · Serdar Ozcelik[3] · Mustafa M. Demir[2] · M. Naci Inci[1]

Received: 9 September 2021 / Accepted: 4 November 2021

Abstract
Strongly concentrated optical fields around a metal nanoparticle in the close vicinity of a dipole noticeably facilitate dramatic changes in the localized density of states due to hybrid photonic–plasmonic mode couplings as compared to that of the pure cavity mode fields. Significant variations of the field intensity in the presence of the metal nanoparticle elucidate enhanced light–matter interaction in a hybrid structure. The enhancement factor of the light–matter interaction is studied through the single-atom cooperativity parameter, which is directly proportional to the ratio of the fluorescence lifetimes of the off-resonant and on-resonant emission. A compact and cost-effective hybrid device, which includes a microfiber cavity, supporting whispering gallery modes, and a well-defined solid nanostructure, consisting of a gold nanoparticle core, overcoated by a silica shell, and decorated with CdS/CdSe quantum dots, is demonstrated to offer an outstanding potential for the enhancement of light–matter interaction. Surface plasmons of a gold nanoparticle, placed inside a hollow cylindrical nanostructure at the surface of a microfiber, are activated upon excitation of the dipoles of the quantum emitters, which are on-resonance with the whispering gallery mode. Time-resolved experiments demonstrate that the single-atom cooperativity parameter of the quantum dots is enhanced by a factor of about 4.8 in the presence of the gold nanoparticle being simultaneously in strong interaction with the cavity mode field and the metal nanoparticle's surface plasmons.

Keywords Light-matter interaction · Hybrid cavity · Gold nanoparticle · Single-atom cooperativity parameter · Cavity mode

1 Introduction

Confinement of the electromagnetic fields into nanoscale regions for an efficient control of light–matter interaction has been at the heart of research in the area of quantum optics, specifically in nanophotonics, nanoplasmonics, and quantum electrodynamics [1–4]. Advances in optical nanotechnologies have enabled to produce many successful dielectric photonic cavities or plasmonic nanostructures to store the optical power temporally or spatially, which result in an enhancement of the density of the electromagnetic states (LDOS) at localized regions [5–9]. Plasmonic particles, which are capable of facilitating extreme enhancement of a local field, have outperformed to overcome the diffraction limit of the dielectric cavities [10–13]. Nevertheless, the intrinsic ohmic loss of the metal particles restricts the use of these noble particles in efficient photonic devices [14]. On the other hand, miniaturization of the dynamic optical devices requires both low energy dissipation and strong optical field density in a resonator for which it has been demonstrated to be possible by integrating plasmonic nanostructures into dielectric photonic environments [15–19]. Although it is challenging to efficiently couple a light beam propagating in the free space into an individual metal nanoparticle directly, the coupling strength of the light emission from a quantum source into the surface plasmons of a metal nanoparticle has been shown to dramatically increase as the plasmonic nanoparticle is placed inside a resonant dielectric cavity and interacting with the optical mode field of the resonant structure [20–23]. Thus, the hybrid photonic–plasmonic modes have been unveiled to be promising for the principal

✉ Belkıs Gökbulut
belkis.gokbulut@boun.edu.tr

[1] Department of Physics, Bogazici University, Bebek, 34342 Istanbul, Turkey

[2] Department of Materials Science and Engineering, Izmir Institute of Technology, Urla, 35430 Izmir, Turkey

[3] Department of Chemistry, Izmir Institute of Technology, Urla, 35430 Izmir, Turkey

Published online: 12 November 2021

studies of the enhanced light–matter interaction because of the outstanding capability of the strong field enhancement of the plasmonic nanoparticles incorporated into the photonic systems [24–28]. All in all, the realization and optical characterization of numerous hybrid photonic–plasmonic devices have been performed to present elegant ways for controlling light–matter interaction and the achievement of the conceptually novel approaches to produce highly efficient nanophotonic devices [29–33]. Particularly, the enhancement of the light–matter interaction in a composite metal nanoparticle–whispering gallery mode (WGM) coupling system was lucidly revealed in a theoretical study [34]. The single-atom cooperativity of a dipole in the hybrid structure was demonstrated to be significantly enhanced in the presence of a metal nanoparticle, compared to that of the bare WGM resonator.

In this paper, the single-atom cooperativity parameter per ensemble of CdS/CdSe quantum dots (QDs) in the close vicinity of a metal nanoparticle, which is integrated into a microfiber resonator, is experimentally and numerically investigated for the first time through time-resolved fluorescence lifetime measurements. Cylindrical nanoholes are formed on the surface of the electrospun polystyrene (PS) microfibers that support WGMs. Gold nanoparticles are coated with a silica layer, decorated with CdS/CdSe QDs to hierarchically synthesize solid Au/SiO_2/QDs nanostructures. This ensures a certain distance between the dipoles of the quantum light sources and the surface plasmons of the metal nanoparticle, as introduced in the theoretical model [34]. Individual QDs and solid Au/SiO_2/QDs nanoparticles are separately placed inside the cylindrical nanoholes of the identical resonant microfibers to explore the purposeful role of the plasmonic nanoparticle integrated into the photonic structure on the enhancement of the light–matter interaction. In the composite structure, as the microfiber cavity serves as a moderate resonator to alter the emission dynamics of the coupled QDs, the gold nanoparticle in the close vicinity of the dipoles enables to generate a hot electromagnetic spot through subwavelength light confinement beyond the diffraction limit, yielding a reproduction of the hybrid photonic–plasmonic mode. Therefore, the interaction between the dipole of the QDs and the optical mode field is considerably enhanced by the synergetic effect of the photonic and plasmonic structures through considerably increased density of the optical states. The fluorescence dynamics of the CdS/CdSe QDs, which are coupled into the pure optical mode and hybrid photonic–plasmonic mode, are explored via fluorescence decay parameters of the coupled quantum light sources. As a result, the light–matter interaction in the resonant microfiber cavity is determined to enhance by a factor of about 4.8 in the presence of a single gold nanoparticle. Thus, the ability to concentrate the electromagnetic waves at nanoscale by making use of a reproducible and stable host photonic structure and a well-defined solid nanoparticle that consists of a gold nanocore and individual QDs, separated by a silica shell, based on a purely chemical synthesis procedure instead of sophisticated engineering techniques, seems to be promising for the noteworthy advances in nanophotonics, quantum information technologies, and revolutionary optical sensing applications. In this regard, we believe that our work is a key step toward the fabrication of polymer-based hybrid photonic–plasmonic devices to enhance the light–matter interaction.

2 Experimental section

2.1 Materials and methods

CdS/CdSe QDs-decorated Au core/SiO_2 shell nanostructures are synthesized with a multistep procedure, which is illustrated in Fig. 1a. The structural composition of a hybrid microfiber structure, which consists of an electrospun polymer microfiber with cylindrical nanoholes, formed on the surface of the microstructure, and QDs-decorated Au core/SiO_2 shell nanostructure, is also demonstrated in Fig. 1b.

2.1.1 Synthesis of spherical gold nanoparticles

Au nanoparticles are synthesized by reducing the Au^{3+} ions. In this purpose, the $HAuCl_4$ (16.3 mg) is dissolved in 200 mL of water and heated up to reflux under vigorous stirring. Next, an aliquot of the solution of trisodium citrate (0.34 M, 1 mL) is added into the boiling system. The mixture is kept under reflux, which provides a reduction; therefore, the color changes into red. The resulting mixture is centrifuged (12,000 rpm, 15 min) and redispersed in water. The Au nanoparticles are coated by adding PVP (21.5 mg) into 45 mL of Au dispersion. The particles are then separated by centrifuge (12,000 rpm, 15 min) and redispersed in 26 mL of ethanol.

2.1.2 *Synthesis of Au Core/SiO_2 shell nanoparticles*

The SiO_2 shells onto Au nanoparticles are synthesized by the sol–gel technique in an alkali medium. The NH_3 (25 µL) is added into PVP-coated Au nanoparticles dispersion (9 mL). Subsequently, TEOS (three equal portions of 20 µL) is injected to start the reaction, which is maintained for 6 days. The surface of Au core/SiO_2 shell nanoparticles is finally modified by –SH groups through mixing the addition of a 20-µL (3-mercaptopropyl) trimethoxysilane for 24 h. The dispersion is centrifuged and redispersed in 3 mL of water. The Dynamic light scattering (DLS) measurement is performed to determine the average size of the Au particles, which is measured to be about 14 nm. The

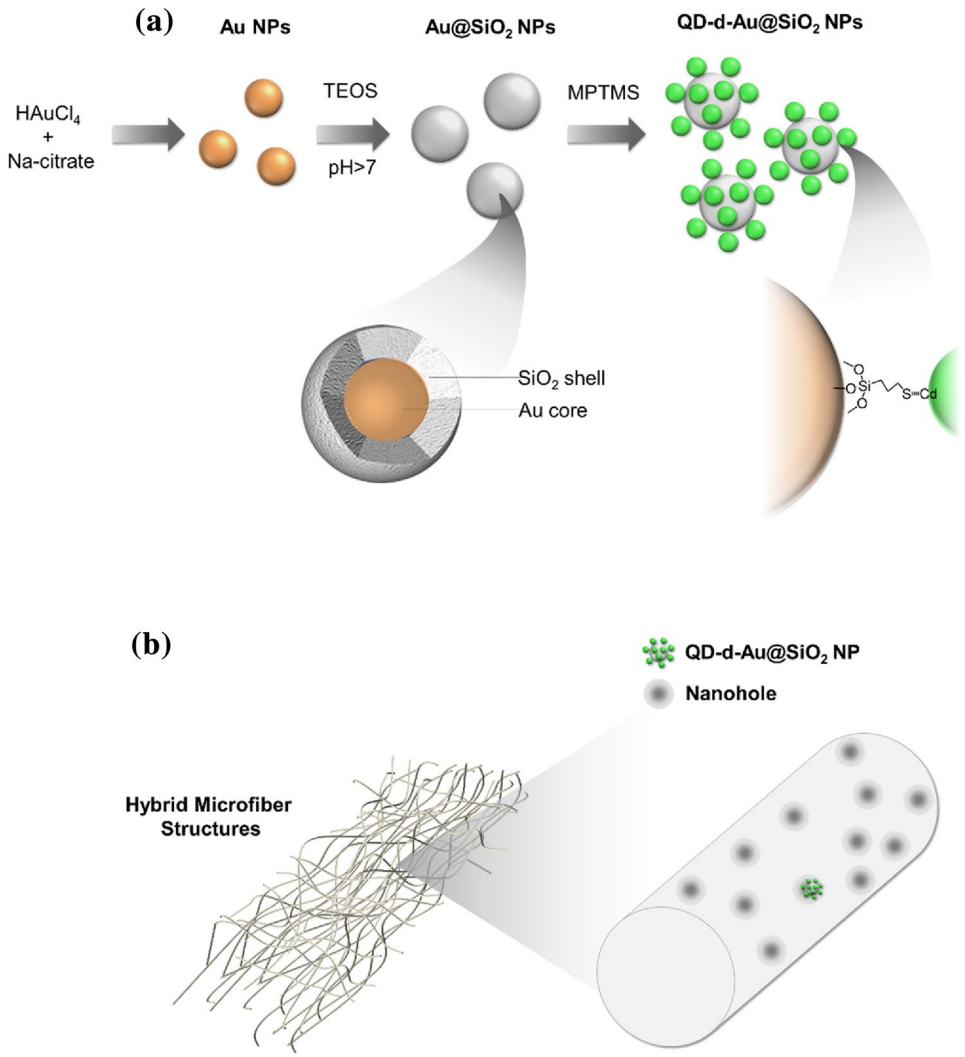

Fig. 1 Schematic representation of **a** multistep synthesis procedure of Au/SiO_2/QDs nanostructures and **b** structural composition of the hybrid microfiber structure, which consists of an electrospun polymer microfiber with cylindrical nanoholes, formed on the surface of the microstructure, and QDs-decorated Au core/SiO_2 shell nanostructure

average size of the synthesized spherical Au nanoparticles in diameters before and after SiO_2 shell formation is given in Fig. 2. The average diameter of the polymer-coated Au nanoparticles is observed to reach a value of about 44 nm, which means that the shell thickness surrounding the gold nanoparticles increases gradually from about 5 nm to 15 nm, as shown in Fig. 2.

Photoluminescence excitation (PLE) and emission spectra of CdS/CdSe QDs together with the PLE spectrum of the Au nanoparticles are given in Fig. 3. An overlap between the photoluminescence excitation spectrum of the Au nanoparticles and the photoluminescence emission spectrum of the QDs is clearly observed in Fig. 3. In a QD–gold nanoparticle system, the gold nanoparticle can behave as the efficient energy acceptor, which is able to quench the fluorescence emission energy of the donor QD, depending on the thickness between these two nanoparticles.

2.1.3 *The fabrication of QDs-decorated Au Core/SiO_2 shell nanostructures*

The CdS/CdSe QDs are easily capped onto Au core/SiO_2 shell nanoparticles since the –SH structures having affinity to Cd. In this wise, both SiO_2 overcoated Au (1 mL) and CdS/CdSe QD (1 mL) dispersions are placed into a glass vial and gently shaken for 1 h. The particles are merged with each other at the toluene/water interface. The organic phase is decanted, and the particles are separated by centrifuge and redispersed in water (1 mL).

The characteristic properties of electrospun polymer microfibers with cylindrical nanoholes, formed on the surface of the microstructure, are given in detail [35]. Scanning electron microscopy (SEM) image of the polymer microfiber with a diameter of about 7 μm, used in our experiments, is demonstrated in Fig. 4a. The integration of QDs and Au/SiO_2/QD particles into the cavities is

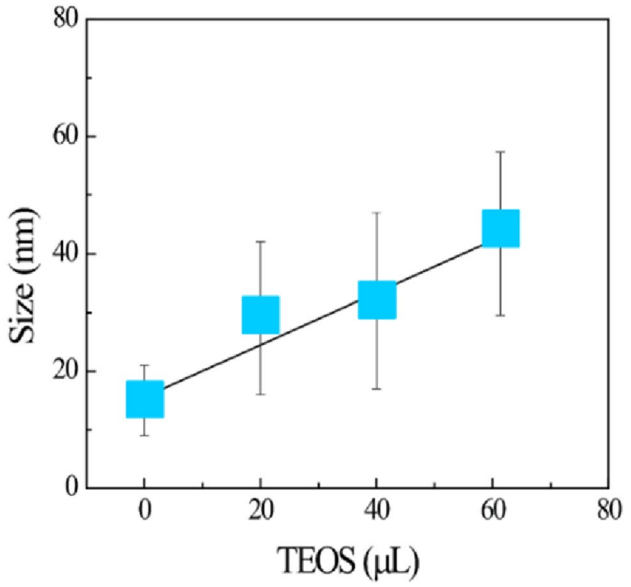

Fig. 2 Diameter vs TEOS concentration of silica layer-coated gold nanoparticles

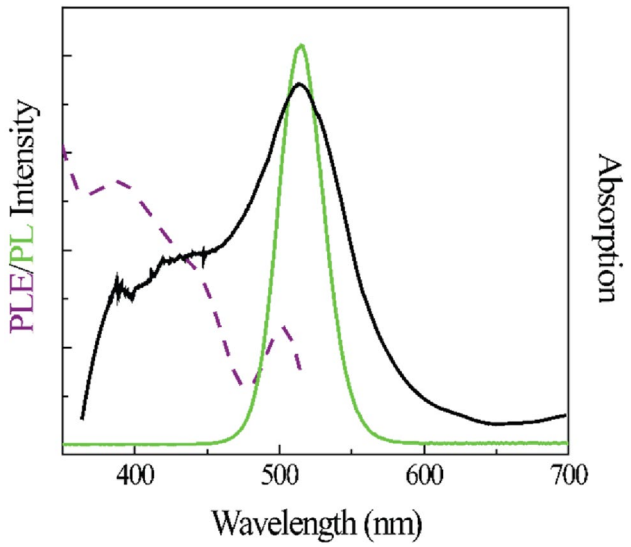

Fig. 3 PLE and PL emission spectra of CdS/CdSe QDs and PLE spectrum of the Au nanoparticles (dashed curve)

achieved by infiltration of the dispersion of the particles through a polymer fiber mat. A very dilute solution of nanoparticles and polystyrene microfibers are placed in a syringe. Then, the dispersion is forced to be filtrated through the fiber mat by pressing the injector. Since the majority of the fiber surface area consists of cylindrical nanoholes, most of the particles are trapped into the nanoholes. SEM images of the individual QDs and solid

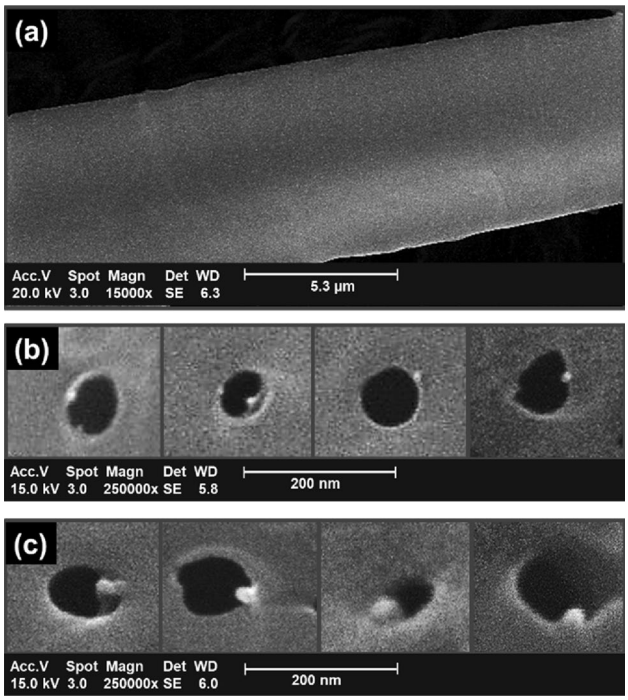

Fig. 4 SEM images of the **a** electrospun polymer microfiber, **b** QDs, and **c** solid Au/SiO_2/QDs nanostructures integrated into the cylindrical nanoholes formed on the surface of the polystyrene microfibers

Au/SiO_2/QDs nanostructures, which are integrated into the cylindrical nanoholes on the surface of the polystyrene microfibers, are also demonstrated in Fig. 4b and c, respectively.

In our samples, since porous microfibers are exposed to a highly diluted QDs concentration, only a few QDs are captured into a nanopore of the microfiber. Similarly, as a hybrid Au/SiO_2/QDs nanoparticle is concerned, which contains only a few QDs, QD concentration for all optical and hybrid microresonators remains almost similar. Therefore, the average value of these nanocrystals, interacting with the optical mode and the hybrid photonic–plasmonic mode, is taken to perform the calculations of the single-atom cooperativity parameter per QD ensemble.

Additionally, only the dipole of the fluorescent quantum source embedded into the pore of the microfiber is able to induce the WGMs since the optical field could exist inside the outer boundary of the polymer microcavity. Thus, the pores of the microstructure, which include the dipoles of the QDs and the hybrid Au/SiO_2/QDs nanoparticles, facilitate the origination of the WGMs and the interaction of the optical mode field with the plasmonic nanoparticle, given the fact that the depth of each pore on the surface of the microfiber, which is about 100–150 nm, is sufficient for the excitation of the hybrid photonic–plasmonic mode field.

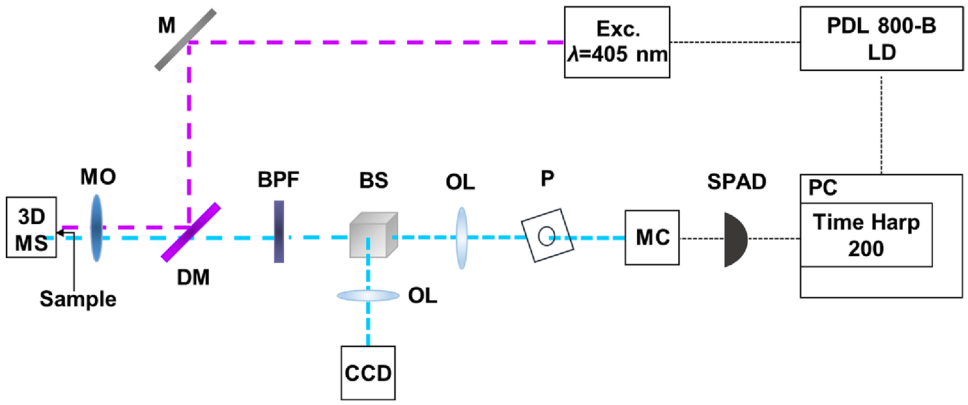

Fig. 5 The illustration of the optical setup used in time-resolved experiments

2.2 Time-resolved fluorescence lifetime measurements

Our time-resolved experiments are performed with the optical setup given in Fig. 5. Fluorescence decay curves of the QDs are obtained by time-correlated single-photon events using Time Harp 200 PC-Board system (PicoQuant, GmbH). A pulsed diode laser with a wavelength of 405 nm (LDH-D-C-405 PicoQuant, GmbH) and PDL 800-B laser driver are operated for the excitation of the fluorescent emitters. A microscope objective (MO) (Nikon ELWD 100X) is employed to focus the laser beam reflecting from the dichroic mirror (DM) to the light emitters and to collect the photoluminescence from the excited QDs. A band-pass optical filter (BPF) and a monochromator are interrogated to eliminate the laser beam and acquire the on-resonant light emission with a desired wavelength interval from the fluorescing signal, respectively. A beam splitter (BS) is used to separate the fluorescence signal through a single-photon avalanche diode photodetector (SPAD) and a CCD camera (Optronis-1836-ST-153) for the measurements of the photon transitions and the observations of the intense electromagnetic field zones upon excitation of the QDs, respectively. Fluorescence lifetimes of the QDs, τ_1, τ_2, and τ_3, amplitude-averaged ($<\tau_a>$) and intensity-averaged (τ_b) lifetimes with their detailed decay parameters, including the fitting parameter (χ^2), are determined by FluoFit computer program, which are given in detail [36].

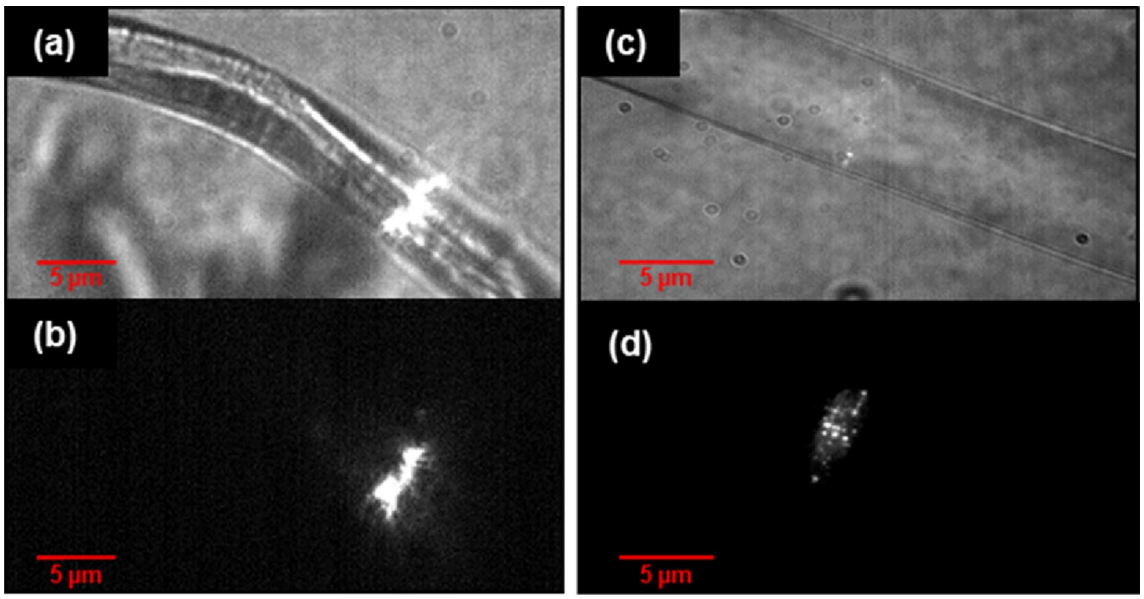

Fig. 6 The confocal images of the microfibers in which the intense electromagnetic field regions originate from **a** the hybrid photonic–plasmonic structure through coupling into the WGM with **b** its dark image when the white light is off and **c** the pure optical mode with **d** its dark image

3 Results and discussion

The confocal images of the resonant microfibers in which the solid Au/SiO_2/QDs nanoparticles and the individual QDs are placed inside the cylindrical hollow nanostructures are obtained through the excitation of the quantum light sources, as given in Fig. 6a, b, c, and d, respectively. The photoluminescence from the individual QDs is directly coupled into the photonic resonator to generate a WGM, which is so called a pure optical mode. On the other hand, the excited dipoles of the QDs, which are chemically attached to the silica layer overcoated gold nanoparticle, interact with the surface plasmons of the metal nanoparticle and the cavity mode field simultaneously to generate a synergetic mode field, which is so called a hybrid photonic–plasmonic mode.

Compared to the confocal images of the photonic resonator that supports a pure optical mode given in Fig. 6c and d, the substantially enhanced fluorescence emission upon interaction of the dipole with the surface plasmons of the gold nanoparticle and the cavity mode field of the resonator, when the white light is on and off, is explicitly observed in the hybrid structure, as seen in the confocal images of Fig. 6a and b, respectively.

The time-resolved experiments are performed based on the observations of the enhanced electromagnetic field regions on the surface of the resonant microstructures. Figure 7 shows the decay curves of the QDs for the following situations: QDs (*i*) on bulk polymer, (*ii*) coupled into the pure optical mode of the cavity; QDs, chemically attached to the Au core/ SiO_2 shell nanoparticles, which are (*iii*) on bulk polymer and (*iv*) coupled into the hybrid photonic–plasmonic mode, with distinctive characteristics of the photon populations. The corresponding decay parameters of the QDs with the fitting equations, including the fitting quality parameters (χ^2), the fluorescence lifetimes of the QDs, τ_1, τ_2, and τ_3 with their percentage values, amplitude-averaged ($<\tau_a>$) and intensity-averaged (τ_b) lifetimes, are also given in detail in Fig. 8. The averaged fluorescence lifetime of the QDs on bulk polymer is measured to be about 21.1 ns. The averaged fluorescence lifetime of the QDs attached to the core/shell–Au/SiO_2 nanoparticles, without being incorporated into the cavity structure, is also measured to be about 13.2 ns, using two exponential decay fits, with lifetimes of 21.5 ns and 6.3 ns. Although the silica layer with a thickness of 15 nm between the surface of the gold nanosphere and the QDs ensures eliminating the majority of the electron and energy transfers between the metal nanoparticle and the light emitters, the averaged fluorescence lifetime of the QDs is affected by the presence of the gold nanoparticle. In such a semiconductor–metal hybrid nanostructure, gold nanoparticles can behave as the efficient energy acceptors and are able to quench the fluorescence emission energy of the donors due to nanosurface energy transfer (NSET) processes. NSET model has emerged as an energy transfer mechanism that can measure gold and fluorescent molecule interactions over distances up to 20 nm. Thus, the reason behind the decreased fluorescence lifetime of QDs attached to the Au core/SiO_2 shell nanostructures on the surface of the bulk polymer can be explained by NSET model. However, as shown in Figs. 7 and 8, when the fluorescence emissions from the QDs and QDs attached to the Au/SiO_2 nanoparticles couple into the mode fields, the decay dynamics of the fluorescent emitters are observed to change considerably. The fluorescence lifetimes of the quantum sources, coupled into the optical and hybrid modes, are also determined by the decay curves shown in Fig. 7, using two and three exponential fits, respectively. The multi-exponential decay populations of the QDs integrated into the photonic cavities include both on-resonant and off-resonant fluorescence emissions from the excited dipoles. In this respect, since the confinement of the electromagnetic waves dramatically enhances the transitions of the photons upon coupling of the light emission into the resonant optical fields, the fastest exponential decay components always account for the on-resonant dipole emissions and the other decay components of the fluorescence signal are attributed to be the light emission coupled into the off-resonant optical modes.

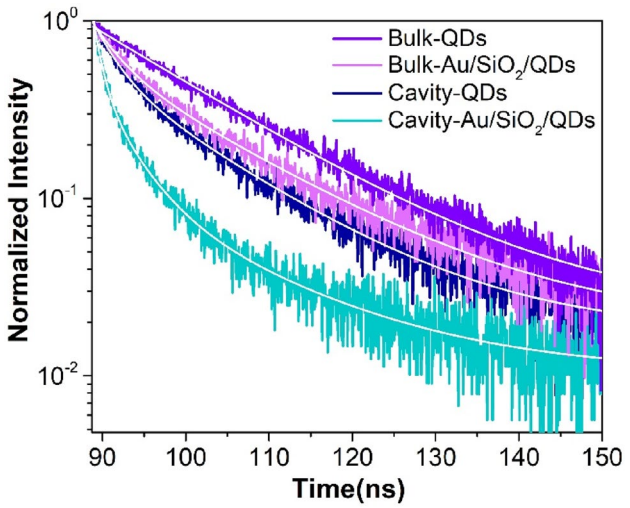

Fig. 7 The fluorescence decay curves of the individual QDs, which are on bulk polymer and coupled into the pure optical mode and the QDs chemically attached to the Au core/SiO_2 shell nanoparticles, which are on bulk polymer and coupled into the hybrid photonic–plasmonic mode

Thus and so, as given in Fig. 8, the second fluorescence lifetime (τ_2) of the QDs, coupled into the pure optical mode, and the third fluorescence lifetime (τ_3) of the QDs attached to the Au/SiO_2 nanoparticles, coupled into the hybrid photonic–plasmonic mode, originate from the confinement of the electromagnetic waves. Our time-resolved measurements

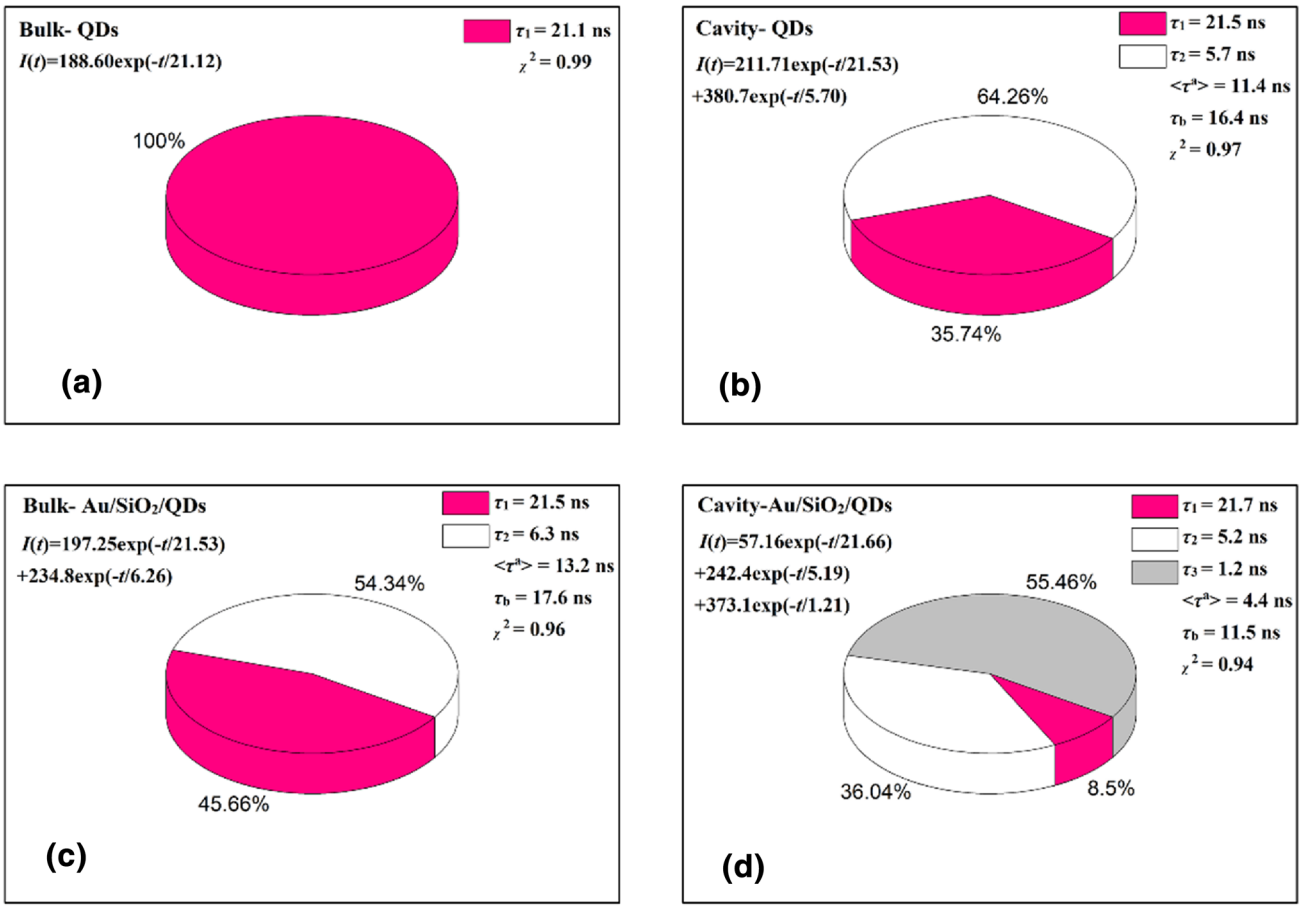

Fig. 8 The decay parameters of the QDs, which are **a** on bulk polymer and **b** coupled into the pure optical mode in addition to the QDs chemically attached to the Au core/SiO_2 shell nanoparticles, which are **c** on bulk polymer and **d** coupled into the hybrid photonic–plasmonic mode, including their fitting equations and parameters (χ^2), the fluorescence lifetimes, τ_1, τ_2, and τ_3 with their percentage values, amplitude-averaged ($<\tau_a>$) and intensity-averaged (τ_b) lifetimes

demonstrate that as the fastest decay lifetime of the quantum light sources coupled into the pure optical mode is determined to be 5.7 ns, the fluorescence lifetime of the QDs coupled into the hybrid photonic–plasmonic mode is measured to be 1.2 ns. The noteworthy change in the characteristics of the fastest decay populations originates from the enhanced density of the electromagnetic states as a result of the redistributed optical mode field upon the strong interaction of the dipole with the localized surface plasmons of the gold nanoparticle along with the WGMs of the microresonator. Additionally, although the NSET mechanism is not completely excluded in our study, the dominant mechanism that affects the fastest decay component of the QDs is assumed to be the mode coupling according to the experimental results.

The single-atom cooperativity parameter of the dipole, C, coupled into the photonic cavity structure, could be obtained by the Purcell enhancement factor, F_p [37], because it is directly proportional to the Purcell factor, which is calculated by the ratio of the fluorescence lifetimes of the off-resonant and on-resonant QDs with a particular optical mode. The enhancement factor of the cooperativity parameter in the presence of the metal nanoparticle, i.e., C_{c+m}/C_c, is experimentally determined by the ratio of the Purcell factors of the fluorescing CdS/CdSe QDs, which are coupled into the pure optical mode (C_c) and the hybrid photonic–plasmonic mode (C_{c+m}) [38]. Since the photon–plasmon coupling efficiency is strongly dependent on the size and morphology of the plasmonic nanostructures and the exact location of the metallic nanoparticles with respect to the dielectric cavities, the enhancement factor of the resonant fluorescent emitters varies for each distinctive hybrid photonic–plasmonic mode coupling [39].

Our time-resolved experimental results reveal that the light–matter interaction is enhanced approximately by a factor of 4.8 upon coupling of the quantum light sources into the hybrid mode, compared to that of the light emitters coupled into the pure WGM resonator. To analyze how much variance is encountered in these hybrid devices, the time-resolved experiments have been performed at five times using the same microcavity with a similar Au/SiO_2/

QDs nanoparticle. Different enhancement factors, ranging from the values of 3.4 to 5.2, have been calculated based on the data obtained from the experiments. The variance of the cooperativity parameter enhancement factor in the presence of the plasmonic nanoparticle, which is defined by $Var(C_{c+m}/C_c) = <(C_{c+m}/C_c)^2> - <(C_{c+m}/C_c)>^2$, is also calculated to be about 0.4. Thus, a statistically significant change of the emission rate has been observed as a result of the coupling of the light emission into the hybrid photonic–plasmonic mode.

The electric field patterns of the CdS/CdSe QDs coupled into the resonant modes and the optical properties of the photonic structures are numerically studied by 3D finite difference time-domain (FDTD) technique. In the simulations, the cylindrical hollow nanostructures, which have diameters ranging from 60 to 150 nm, are embedded to the surface of the PS matrix of a resonant microfiber. Electric dipoles and Au core/SiO_2 shell nanoparticles are placed inside the hollow nanostructures of the resonant microfibers. The material properties of the PS matrix, a gold nanosphere with a diameter of about 14 nm, and a surrounding silica layer with a thickness of 15 nm are utilized in the numerical calculations.

The numerically obtained simulation results of the electric field distribution profiles of the dipole of the QD coupled into the pure WGM and the dipole of the fluorescing QD attached to the Au core/SiO_2 shell nanostructure, coupled into the hybrid photonic–plasmonic mode of the microfiber resonator, are given in Fig. 9a and b, respectively. The zoomed electric field distribution profile of the dipole surrounding the Au core/SiO_2 shell nanostructure, embedded inside the microfiber resonator, as illustrated in the white colored rectangular frame in Fig. 9b, is also given in Fig. 9c. The strongly concentrated optical field around the gold nanoparticle in the close vicinity of the dipole clearly demonstrates the dramatic change in the LDOS upon hybrid

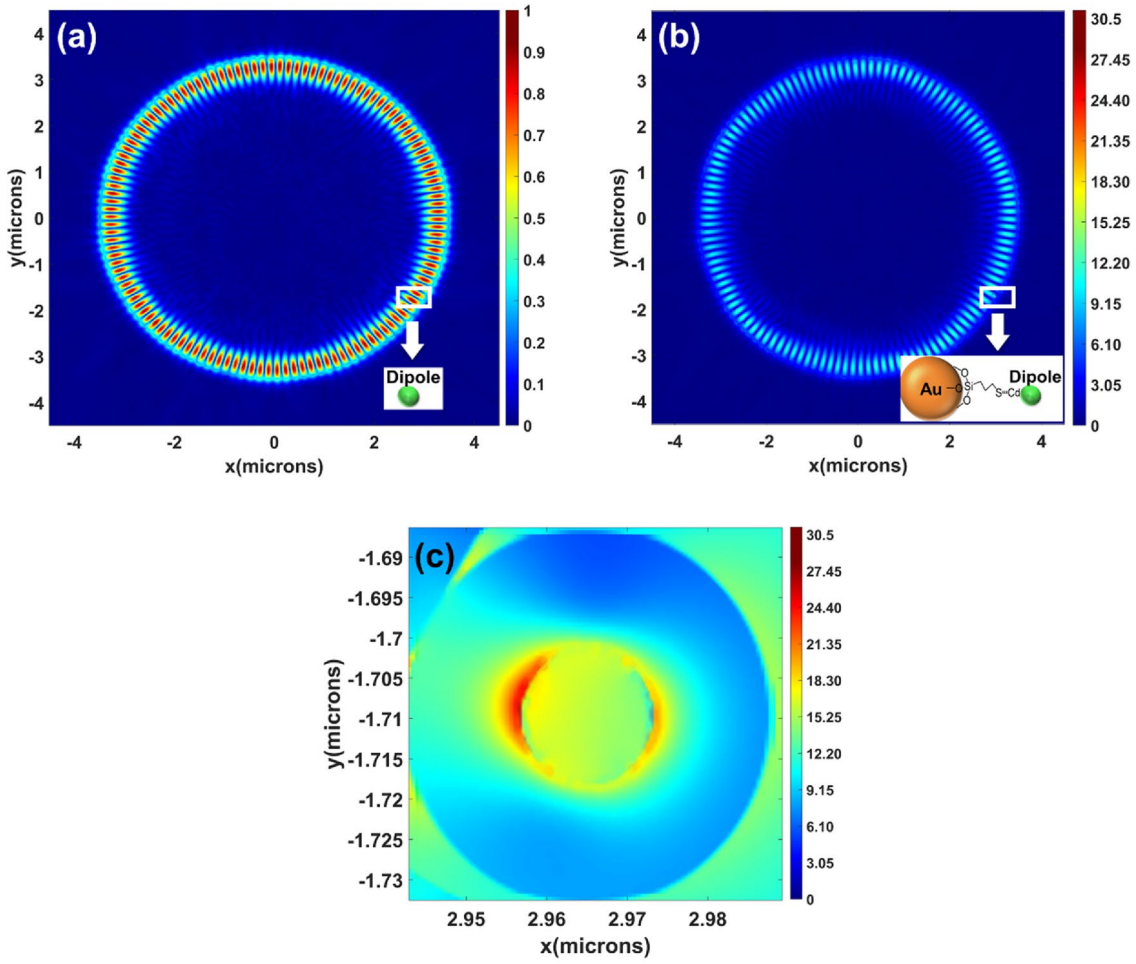

Fig. 9 Numerically obtained cross-sectional electric field distribution profiles of the dipoles of the QDs coupled into **a** the pure WGM and **b** the hybrid photonic–plasmonic mode of the microfiber resonators, with a diameter of 7 μm. **c** The electric field distribution profile of the dipole surrounding the Au core/SiO_2 shell nanostructure, which is placed inside the hollow cylindrical nanostructure at the surface of a microfiber resonator

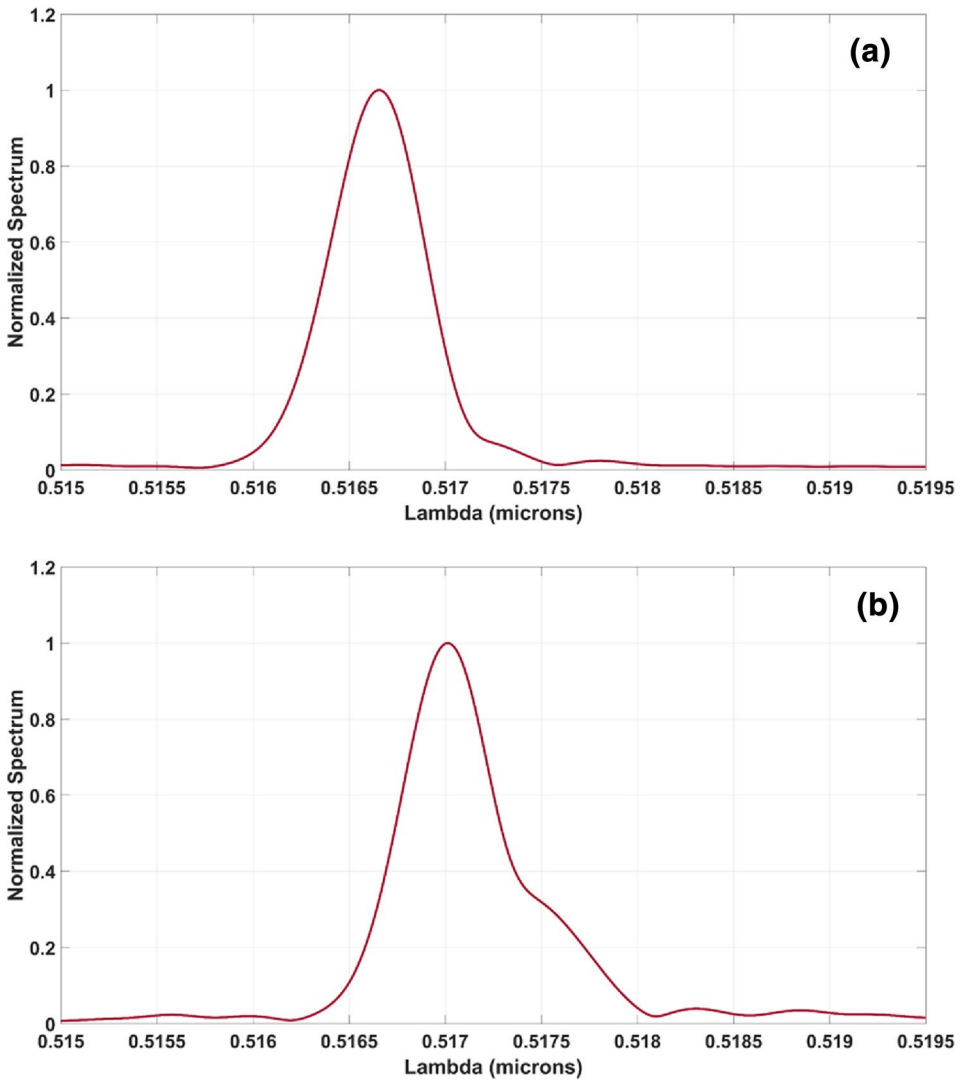

Fig. 10 The photoluminescence spectra of the dipoles coupled into the **a** pure optical mode and **b** hybrid photonic–plasmonic mode of the microresonators

photonic–plasmonic mode coupling when compared to that of the pure cavity mode field. This variation of the field intensity in the presence of the gold nanoparticle elucidates the enhanced light–matter interaction in the hybrid structure.

Figure 10 shows the obtained fluorescence emission spectra of the dipoles coupled into the pure optical mode and the hybrid photonic–plasmonic mode for microresonators with a diameter of 7 μm in which a shift in the resonant wavelength of the microstructure occurs in the presence of the plasmonic nanoparticle. It is well known that a shift of a resonant frequency of a microcavity mode, induced by a perturbing effect of a single gold nanoparticle, is determined by Bethe–Schwinger cavity perturbation formula in which an illuminated volume of the cavity structure and the volume of the gold nanoparticle play a crucial role [40]. Particularly, any perturbation in the optical path length of the coupled light emission into the WGM resonators, owing to their high sensitivity to surrounding medium, is expected to result in a significant shift of the resonant frequency of the optical mode [41]. In our study, when the gold nanoparticle interacts with the extending evanescent field of the WGM, it causes the frequency of the resonant mode to shift while enhancing the local evanescent field. However, since the volume of the core/shell nanostructure is too small, compared to the illuminated volume of the cavity structure, a slight shift in the resonant wavelength of the WGM is observed, as shown in Fig. 10.

WGM-based microresonators, similar to the cylindrical microcavity proposed in our study, have a pair of degenerate modes in opposite propagation directions with the same resonant frequency and the field distribution. These propagating modes are called clockwise and counterclockwise WGMs. Any perturbation in the microresonator such as material inhomogeneity or a scatterer, interacting with the WGM, induces the degenerate modes to split into a double mode with different frequencies [42]. In our study, first of all, when randomly distributed cylindrical nanoholes are formed on the surface of the microresonator, the symmetry

is naturally broken to yield a mode splitting as demonstrated with an indistinct emission peak in addition to the main resonant peak at the wavelength of around 0.5167 microns, as shown in Fig. 10a. As the core/shell–Au/SiO_2 nanoparticle, which acts like a scatterer, is integrated into the nanohole, the split mode at the wavelength of around 0.5175 microns is observed to be enhanced as a result of the perturbation, as shown in Fig. 10b.

The enhancement factor of the light–matter interaction is determined by the calculations of the single-atom cooperativity parameter based on the theoretical approach using Eq. 1 [43]:

$$C = \frac{2G^2}{\kappa\gamma_s}, \tag{1}$$

where γ_s is the spontaneous decay of the quantum light source; κ is the decay of the cavity mode field, which is determined by the ratio of the frequency and the quality factor of the cavity mode (ω_c/Q); and G is the single-photon coupling strength, which is defined by

$$G = \mu f_c(\mathbf{R})\left(\frac{\omega_c}{(2\hbar\varepsilon_0\varepsilon_c V_c)}\right)^{1/2}, \tag{2}$$

in which ε_0 represents the permittivity of the vacuum; ε_c and μ indicate the permittivity and permeability parameters of the cavity structure, respectively; $f_c(\mathbf{R})$ is the normalized field distribution in the photonic structure at a distance R; and V_c is the mode volume of the resonant optical cavity, which is calculated by integrating the electric field intensity of the cavity mode over a volume and normalizing it to the maximum field intensity. Nevertheless, since the gold nanoparticle integrated into the resonant cavity causes a radiation leakage, the definition of the mode volume is revised by considering both real and imaginary parts, which corresponds to be the confined optical mode field and the energy loss from the cavity, respectively. Thus, the revised form of the mode volume using the total electromagnetic field ($\tilde{\mathbf{E}}, \tilde{\mathbf{H}}$) produced by a linearly polarized dipole, $\boldsymbol{p} = pu$, with a unit vector, $\boldsymbol{u}$, is utilized in the numerical calculations as given by Eq. 3 [44]:

$$V = \frac{\int\left[\tilde{\mathbf{E}}\cdot\frac{\partial(\omega\varepsilon_c)}{\partial\omega}\tilde{\mathbf{E}} - \tilde{\mathbf{H}}\cdot\frac{\partial(\omega\mu)}{\partial\omega}\tilde{\mathbf{H}}\right]d^3\mathbf{r}}{2\varepsilon_0 n^2\left[\tilde{\mathbf{E}}(\mathbf{r}_0)\cdot\mathbf{u}\right]^2}. \tag{3}$$

The mode volume and the Q-factor of the pure WGM resonator with a specific diameter of 7 μm are acquired to be 3.67×10^{-19} m^3 and 464 ± 22, respectively, based on our numerical calculations. On the other hand, the hybrid photonic–plasmonic system with the same diameter of the resonant microfiber is observed to give a mode volume of 2.71×10^{-20} m^3 along with the imaginary part of -1.73×10^{-25} m^3 and a Q-factor of 471 ± 24. The absorptive nature of the gold nanoparticle, integrated into the microcavity structure, causes the Q-factor of the resonant mode to decrease because of the radiation loss on the surface of the metal nanoparticle. Nevertheless, in our study, using a gold nanoparticle with a diameter of 14 nm minimizes the decrease in the Q-factor of the optical mode, which is observed to be in the error margin of the numerical results. The enhancement of the light–matter interaction is theoretically calculated by the ratio of the single-atom cooperativity parameters of the QDs coupled into the pure optical mode and the photonic–plasmonic mode (C_{c+m}/C_c), making use of the numerically obtained parameters of the pure optical and photonic–plasmonic systems. The enhancement factor of the cooperativity parameter of the dipole in the close vicinity of the gold nanoparticle is numerically calculated to be about 13 for the simulated structure, demonstrated in Fig. 9b. Nevertheless, since the photon–plasmon coupling efficiency is strongly dependent on the exact location of the metallic nanoparticles with respect to the dielectric cavities and the location of the dipoles, the enhancement factor of the fluorescent emitters varies for each distinctive hybrid photonic–plasmonic mode coupling in the simulations.

In our experiments, the QDs and QDs-decorated Au core/SiO_2 shell nanostructures embedded into the nanoholes of the microcavity are monitored by SEM images (Fig. 4) to excite the optical and hybrid mode fields. Thus, the exact positions of the nanostructures with respect to the dielectric cavity are quantified from the SEM images and used as an input parameter in the simulations to calculate the enhancement factor numerically. There is a significant dependence of the enhancement factor of the single-atom cooperativity parameter on the QD's position relative to the field maximum. Thus, since the QDs and the QDs attached to the core/shell–Au/SiO_2 nanoparticles are placed inside the nanoholes of the microcavity, the depth of the nanohole is indirectly dependent on the light–matter coupling strength. Increasing the depth of the nanohole toward the field maximum boosts the dipole's interaction with the resonator as long as an overlap of the field maximum and the location of the dipole is well maintained. The numerical calculations have been performed for different hole depths (l) of 100, 150, 200, 250, 300, and 350 nm, to investigate the distance dependence of the enhancement of light–matter interaction with respect to the field maximum. The results are given in Fig. 11a, which indicate that the enhancement factor of the cooperativity parameter is observed to be maximized with the hole depth interval of 200–250 nm and to be decreased as the location of the dipole become distant with respect to the field maximum after the hole depth value of 250 nm.

The layer thickness between the dipole of the quantum light source and the surface plasmons of the metal nanoparticle has also a crucial role on the light–matter interaction. In general, although a shorter layer thickness between the

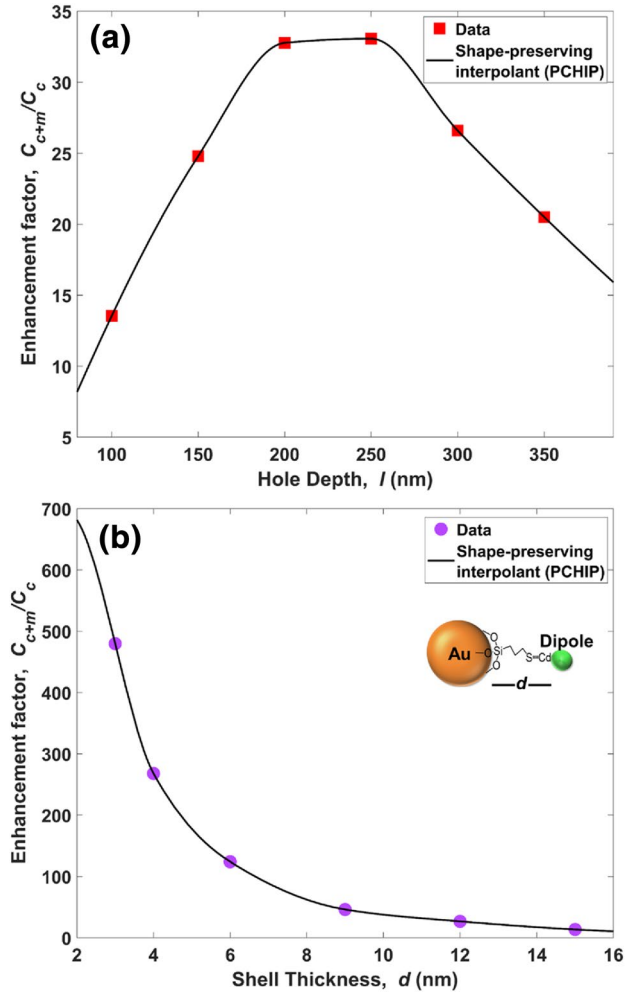

Fig. 11 The numerical results of single-atom cooperativity parameter enhancement factors based on **a** different hole depths (l) of 100, 150, 200, 250, 300, and 350 nm, **b** different silica layer thicknesses (d) of 3, 4, 6, 9, 12, and 15 nm

fluorescent emitters and the gold nanocore is expected to result in a substantially higher enhancement of light–matter interaction [34], it may complicate the fluorescence decay dynamics because of the dominant electron and energy transfer mechanisms between the QDs and the gold nanoparticle [45]. In our study, the silica layer with a controllable thickness between semiconductor and metal nanoparticles offers a well-established photonic platform to eliminate the majority of the electron and energy transfers between the metal nanoparticle and the light emitters. Thus, although numerical calculations have been performed with different silica thicknesses to explore the layer thickness dependence of the cooperativity parameter, the experimental studies have only been performed by QDs attached to the core/shell–Au/SiO_2 nanoparticles with an optimized thickness of the silica layer of 15 nm to focus on the enhancement of the light–matter interaction. Numerical results of the single-atom cooperativity parameter enhancement factors based on different silica layer thicknesses (d) of 3, 4, 6, 9, 12, and 15 nm are given in Fig. 11b. The results unveil the critical importance of the layer thickness between the dipole and the plasmonic nanoparticle as the light–matter interaction is concerned. The coupling of the QDs with hybrid photonic–plasmonic modes is observed to be maximized with the shorter layer thickness of 3 nm between the dipole and the gold nanoparticle, as demonstrated in Fig. 11b.

To compare our experimentally obtained results with the theoretical results of the study aforementioned in "Introduction" section of this paper [34], the diameter of the gold nanosphere is taken to be about 14 nm and the distance between the dipole and the metal surface is specified to be 15 nm to calculate the enhancement of the light–matter interaction upon coupling of the dipole into the hybrid optical mode compared to that of the pure optical mode. An enhancement factor of 5 is unveiled in the presence of the gold nanoparticle [34], which is in a very good agreement with our time-resolved experimental results and calculations.

In recent years, high-performance photonic–plasmonic devices, which are based on photonic resonators and individual plasmonic nanostructures, owing to strong energy storage capacity and high spatial field localization simultaneously, have received a considerable research interest since integrating the metal nanoparticles into the photonic systems offers an outstanding platform for the strong light–matter interaction through the extreme enhancement of the local field [46]. Such hybrid optical modes have also been elucidated to provide an unprecedented optical sensitivity, boosting the performance of the nanophotonic devices [47]. For example, a photonic crystal cavity coupled to a metal nanoantenna was introduced to possess a strong efficiency for photonic trapping by making use of some remarkable optical properties [48, 49]. Moreover, hybridizing WGMs and plasmonic resonances in compact photonic–plasmonic devices were unveiled to have controllable optical sensitivity for biological applications based on wavelength detuning between the WGMs and the plasmonic resonance [50, 51].

In addition to all these, photonic–plasmonic structures consisting of gold nanoantennas in 2D polymer templates with randomly dispersed QDs were demonstrated to have an ability to control the emission intensity and the lifetime anisotropy of the QDs through tailoring the LDOS in the photonic–plasmonic templates [52]. A substantial change in the LDOS upon coupling the light emission from the dipole of the emitter into the hybrid mode field was also reported to significantly alter the fluorescence decay curves and the optical properties of the quantum light sources using opto-plasmonic hybrid materials with tunable photonic–plasmonic properties [53]. Even in a low-Q hybrid photonic–plasmonic resonator, presented by our recent study [54], which comprises a QDs-doped electrospun polymer

nanofiber, partially coated with gold nanoparticles, the spontaneous emission rate enhancement factor of 11.2 was achieved. The results revealed that an increase of about three times in the emission decay rate of the QDs embedded in gold nanoparticles-decorated nanofibers was accomplished compared to those embedded in uncoated ones [54]. In addition to the studies in which the cavities and plasmons are successively combined [20–23], greater enhancement factors of a total emission rate from plasmonic devices [55] and cavities [56], where the fabrication processes are straightforward, have also been demonstrated. In the current study, the surface plasmons of a gold nanoparticle placed inside a hollow cylindrical nanostructure of the resonant microfiber are activated upon excitation of the dipoles of the light emitters, which are on-resonance with the cavity mode field. This yields an enhanced single-atom cooperativity parameter as a result of the regenerated strong optical mode field. Our results demonstrate that a plasmonic nanoparticle, separated by the dipole of the QDs with a desired thickness of a silica layer, enables a controllable light–matter interaction using a hybrid photonic–plasmonic device. Thus, based on a purely chemical synthesis procedure instead of some sophisticated engineering techniques, a compact and cost-effective hybrid device is demonstrated to offer an outstanding potential on the enhancement of the light–matter interaction.

4 Conclusion

In this paper, individual QDs and solid Au/SiO_2/QDs nanoparticles are separately integrated into the cylindrical nanoholes, formed on the surface of the resonant microfibers. The fluorescence dynamics of the CdS/CdSe QDs, which are coupled into the pure optical mode and the hybrid photonic–plasmonic mode, are investigated by a time-resolved spectroscopic technique. The single-atom cooperativity parameter is demonstrated to be enhanced by a factor of 4.8 in the presence of the gold nanoparticle, yielding a strongly enhanced light–matter interaction in the hybrid photonic–plasmonic resonator.

Funding Dr Belkıs Gökbulut acknowledges TUBITAK for the financial support provided under Contract Number 120F323.

Data availability All the required information is presented in the manuscript; further clarifications are available from the corresponding author upon a reasonable request.

Declarations

Conflict of interest The authors declare that they have no conflict of interest.

References

1. Y. Xu, D. Ji, H. Song, N. Zhang, Y. Hu, T.D. Anthopoulos, E.M. Di Fabrizio, S. Xiao, Q. Gan, Light–matter interaction within extreme dimensions: From nanomanufacturing to applications. Adv. Opt. Mater. **6**, 1800444 (2018)
2. A.F. Koenderink, A. Alù, A. Polman, Nanophotonics: shrinking light-based technology. Science **348**, 516–521 (2015)
3. V. Giannini, A.I. Fernández-Domínguez, Y. Sonnefraud, T. Roschuk, R. Fernández-García, S.A. Maier, Controlling light localization and light–matter interactions with nanoplasmonics. Small **6**, 2498–2507 (2010)
4. B. Gökbulut, M.N. Inci, Inhibition of spontaneous emission in a leaky mode wedge nanocavity. Photonics Nanostruct. Fundam. Appl. **32**, 68–73 (2018)
5. S. Combrié, G. Lehoucq, G. Moille, A. Martin, A. De Rossi, Comb of high-Q resonances in a compact photonic cavity. Laser Photonics Rev. **11**, 1700099 (2017)
6. D.S. Dovzhenko, S.V. Ryabchuk, Y.P. Rakovich, I.R. Nabiev, Light–matter interaction in the strong coupling regime: configurations, conditions, and applications. Nanoscale **10**, 3589–3605 (2018)
7. B. Gökbulut, M.N. Inci, Enhancement of the spontaneous emission rate of Rhodamine 6G molecules coupled into transverse Anderson localized modes in a wedge-type optical waveguide. Opt. Express **27**, 15996–16011 (2019)
8. P. Vasa, C. Lienau, Strong light–matter interaction in quantum emitter/metal hybrid nanostructures. ACS Photonics **5**, 2–23 (2018)
9. R.J. Moerland, I.G.C. Weppelman, M. Scotuzzi, J.P. Hoogenboom, Nanoscale imaging of light-matter coupling inside metal-coated cavities with a pulsed electron beam. Nano Lett. **18**, 6107–6112 (2018)
10. D.K. Gramotnev, S.I. Bozhevolnyi, Plasmonics beyond the diffraction limit. Nat. Photonics **4**, 83–91 (2010)
11. D.K. Gramotnev, S.I. Bozhevolnyi, Nanofocusing of electromagnetic radiation. Nat. Photonics **8**, 14–23 (2014)
12. M. Song, C. Wang, Z. Zhao, M. Pu, L. Liu, W. Zhang, H. Yub, X. Luo, Nanofocusing beyond the near-field diffraction limit via plasmonic Fano resonance. Nanoscale **8**, 1635–1641 (2016)
13. S. Raza, N. Stenger, A. Pors, T. Holmgaard, S. Kadkhodazadeh, J.B. Wagner, K. Pedersen, M. Wubs, S.I. Bozhevolnyi, N.A. Mortensen, Extremely confined gap surface-plasmon modes excited by electrons. Nat. Commun. **5**, 4125 (2014)
14. J.A. Schuller, E.S. Barnard, W. Cai, Y.C. Jun, J.S. White, M.L. Brongersma, Plasmonics for extreme light concentration and manipulation. Nat. Mater. **9**, 193–204 (2010)
15. A. Melikyan, L. Alloatti, A. Muslija, D.P. Hillerkuss, C. Schindler, J. Li, R. Palmer, D. Korn, S. Muehlbrandt, D. Van Thourhout, B. Chen, R. Dinu, M. Sommer, C. Koos, M. Kohl, W. Freude, J. Leuthold, High-speed plasmonic phase modulators. Nat. Photon. **8**, 229–233 (2014)
16. V.J. Sorger, N.D. Lanzillotti-Kimura, R.-M. Ma, X. Zhang, Ultra-compact silicon nanophotonic modulator with broadband response. Nanophoton **1**, 17–22 (2012)
17. X. Sun, L. Zhou, H. Zhu, Q. Wu, X. Li, J. Chen, Design and analysis of a miniature intensity modulator based on a silicon-polymer-metal hybrid plasmonic waveguide. IEEE Photonics J. **6**, 4801110 (2014)
18. P. Markov, K. Appavoo, R.F. Haglund, S.M. Weiss, Hybrid Si-VO_2-Au optical modulator based on near-field plasmonic coupling. Opt. Express **23**, 6878–6887 (2015)
19. B. Chen, R. Bruck, D. Traviss, A.Z. Khokhar, S. Reynolds, D.J. Thomson, G.Z. Mashanovich, G.T. Reed, O.L. Muskens, Hybrid

photon–plasmon coupling and ultrafast control of nanoantennas on a silicon photonic chip. Nano Lett. **18**, 610–617 (2018)
20. G. Lv, J. Li, S.-L. Tie, S. Lan, Influence of a three-dimensional photonic crystal on the plasmonic properties of gold nanorods. Opt. Express **24**, 14124 (2016)
21. P. Wang, Y. Wang, Z. Yang, X. Guo, X. Lin, X.-C. Yu, Y.-F. Xiao, W. Fang, L. Zhang, G. Lu, Single-band 2-nm-line-width plasmon resonance in a strongly coupled Au nanorod. Nano Lett. **15**, 7581–7586 (2015)
22. Y. Yin, S. Li, S. Böttner, F. Yuan, S. Giudicatti, E. Saei Ghareh Naz, L. Ma, O.G. Schmidt, Localized surface plasmons selectively coupled to resonant light in tubular microcavities. Phys. Rev. Lett. **116**, 253904 (2016)
23. T. Zhang, M. Wang, Y. Yang, F. Fan, T. Lee, H. Liua, D. Xiang, An on-chip hybrid plasmonic light steering concentrator with ~96% coupling efficiency. Nanoscale **10**, 5097–5104 (2018)
24. P. Peng, Y.-C. Liu, D. Xu, Q.-T. Cao, G. Lu, Q. Gong, Y.-F. Xiao, Enhancing coherent light-matter interactions through microcavity-engineered plasmonic resonances. Phy. Rev. Lett. **119**, 233901 (2017)
25. Y. Yu, T.-H. Xiao, Z.-Y. Li, Optical interaction between one-dimensional fiber photonic crystal microcavity and gold nanorod. Chinese Phys. B **27**, 017301 (2018)
26. T.Y. Kang, W. Lee, H. Ahn, D.-M. Shin, C.-S. Kim, J.-W. Oh, D. Kim, K. Kim, Plasmon-coupled whispering gallery modes on nanodisk arrays for signal enhancements. Sci. Rep. **7**, 11737 (2017)
27. Y. Yin, Y. Chen, E.S.G. Naz, X. Lu, S. Li, V. Engemaier, L. Ma, O.G. Schmidt, Silver nanocap enabled conversion and tuning of hybrid photon–plasmon modes in microtubular cavities. ACS Photonics **4**, 736–740 (2017)
28. S.I. Shopova, C.W. Blackledge, A.T. Rosenberger, Enhanced evanescent coupling to whispering-gallery modes due to gold nanorods grown on the microresonator surface. Appl. Phys. B **93**, 183–187 (2018)
29. B. Barth, S. Schietinger, S. Fischer, J. Becker, N. Nüsse, T. Aichele, B. Löchel, C. Sönnichsen, O. Benson, Nanoassembled plasmonic-photonic hybrid cavity for tailored light-matter coupling. Nano Lett. **17**, 891–895 (2010)
30. W. Ahn, S.V. Boriskina, Y. Hong, B.M. Reinhard, Photonic–plasmonic mode coupling in on-chip integrated optoplasmonic molecules. ACS Nano **6**, 951–960 (2012)
31. J.-N. Liu, Q. Huang, K.-K. Liu, S. Singamaneni, B.T. Cunninghan, Nanoantenna−microcavity hybrids with highly cooperative plasmonic−photonic coupling. Nano Lett. **17**, 7569–7577 (2017)
32. A. Rottler, M. Harland, M. Bröll, M. Klingbeil, J. Ehlermann, S. Mendach, High-Q hybrid plasmon-photon modes in a bottle resonator realized with a silver-coated glass fiber with a varying diameter. Phys. Rev. Lett. **111**, 253901 (2013)
33. A.E. Eter, T. Grosjean, P. Viktorovitch, X. Letartre, T. Benyattou, F.I. Baida, Huge light-enhancement by coupling a bowtie nanoantenna's plasmonic resonance to a photonic crystal mode. Opt. Express **22**, 14464–14472 (2014)
34. Y.-F. Xiao, Y.-C. Liu, B.-B. Li, Y.-L. Chen, Y. Li, Q. Gong, Strongly enhanced light-matter interaction in a hybrid photonic-plasmonic resonator. Phys. Rev. A **85**, 031805(R) (2012)
35. T. Isık, M.M. Demir, Tailored electrospun fibers from waste polystyrene for high oil adsorption. Sustain. Mat. Tech. **18**, e00084 (2018)
36. B. Gökbulut, E. Yartasi, E. Sunar, O.I. Kalaoglu-Altan, T.N. Gevrek, A. Sanyal, M.N. Inci, Humidity induced inhibition and enhancement of spontaneous emission of dye molecules in a single PEG nanofiber. Opt. Mater. Express **8**, 568–580 (2018)
37. T.D. Barrett, T.H. Doherty, A. Kuhn, Pushing Purcell enhancement beyond its limits. New J. Phys. **22**, 063013 (2020)
38. A. Kuhn, D. Ljunggren, Cavity-based single-photon sources. Contemp. Phys. **51**, 289–313 (2010)
39. Y. Yin, J. Wang, X. Lu, Q. Hao, E.S.G. Naz, C. Cheng, L. Ma, O.G. Schmidt, In situ generation of plasmonic nanoparticles for manipulating photon−plasmon coupling in microtube cavities. ACS Nano **12**, 3726–3732 (2018)
40. A. Mitra, H. Harutyunyan, S. Palomba, L. Novotny, Tuning the cavity modes of a Fabry-Perot resonator using gold nanoparticles. Opt. Lett. **35**, 953–955 (2010)
41. I. Brice, K. Grundsteins, A. Atvars, J. Alnis, R. Viter, A. Ramanavicius, Whispering gallery mode resonator and glucose oxidase based glucose biosensor. Sens. Actuat. B Chem. **318**, 128004 (2020)
42. J. Zhu, S.K. Ozdemir, Y.-F. Xiao, L. Li, L. He, D.-R. Chen, L. Yang, On-chip single nanoparticle detection and sizing by mode splitting in an ultrahigh-Q microresonator. Nat. Photonics **4**, 46–49 (2010)
43. D.F. Walls, G.J. Milburn, *Quantum Optics*, 2nd edn. (Springer, Berlin, 2008)
44. C. Sauvan, J.P. Hugonin, I.S. Maksymov, P. Lalanne, Theory of the spontaneous optical emission of nanosize photonic and plasmon resonators. Phys. Rev. Lett. **110**, 237401 (2013)
45. W. Zhu, R. Esteban, A.G. Borisov, J.J. Baumberg, P. Nordlander, H.J. Lezec, J. Aizpurua, K.B. Crozier, Quantum mechanical effects in plasmonic structures with subnanometre gaps. Nat. Commun. **7**, 11495 (2016)
46. O. Benson, Assembly of hybrid photonic architectures from nanophotonic constituents. Nature **480**, 193–199 (2011)
47. M. Chamanzar, A. Adibi, Hybrid nanoplasmonic-photonic resonators for efficient coupling of light to single plasmonic nanoresonators. Opt. Express **19**, 22292–22304 (2011)
48. D. Conteduca, C. Reardon, M.G. Scullion, F. Dell'Olio, M.N. Armenise, T.F. Krauss, C. Ciminelli, Ultra-high Q/V hybrid cavity for strong light-matter interaction. APL Photonics **2**, 086101 (2017)
49. M. Mossayebi, A. Parini, A.J. Wright, M.G. Somekh, G. Bellanca, E.C. Larkins, Hybrid photonic-plasmonic platform for high-throughput single-molecule studies. Opt. Mater. Express **9**, 2511–2522 (2019)
50. C. Klusmann, R.N.S. Suryadharma, J. Oppermann, C. Rockstuhl, H. Kalt, Hybridizing whispering gallery modes and plasmonic resonances in a photonic metadevice for biosensing applications. J. Opt. Soc. Am. B **34**, D46–D55 (2017)
51. A. Bozzola, S. Perotto, F. De Angelis, Hybrid plasmonic-photonic whispering gallery mode resonators for sensing: a critical review. Analyst **142**, 883–898 (2017)
52. C. Indukuri, A. Mukherjee, J.K. Basu, Tailoring local density of optical states to control emission intensity and anisotropy of quantum dots in hybrid photonic-plasmonic templates. Appl. Phys. Lett. **106**, 131111 (2015)
53. Y. Hong, W. Ahn, S.V. Boriskina, X. Zhao, B.M. Reinhard, Directed assembly of optoplasmonic hybrid materials with tunable photonic–plasmonic properties. J. Phys. Chem. Lett. **6**, 2056–2064 (2015)
54. B. Gökbulut, A. Inanç, G. Topcu, S.S. Unluturk, S. Ozcelik, M.M. Demir, M.N. Inci, Enhanced spontaneous emission rate in a low-Q hybrid photonic-plasmonic nanoresonator. J. Phys. Chem. C **132**, 19862–19870 (2019)
55. G.M. Akselrod, C. Argyropoulos, T.B. Hoang, C. Ciracì, C. Fang, J. Huang, D.R. Smith, M.H. Mikkelsen, Nat. Photonics **8**, 835–840 (2014)
56. S. Ek, P. Lunnemann, Y. Chen, E. Semenova, K. Yvind, J. Mork, Slow-light-enhanced gain in active photonic crystal waveguides. Nat. Commun. **5**, 5039 (2014)